

Study of Contact Electrification at Liquid-Gas Interface

Fan Wang, Peng Yang, Xinglin Tao, Yuxiang Shi, Shuyao Li, Zhaoqi Liu, Xiangyu Chen,* and Zhong Lin Wang*



Cite This: <https://doi.org/10.1021/acsnano.1c07158>



Read Online

ACCESS |



Metrics & More



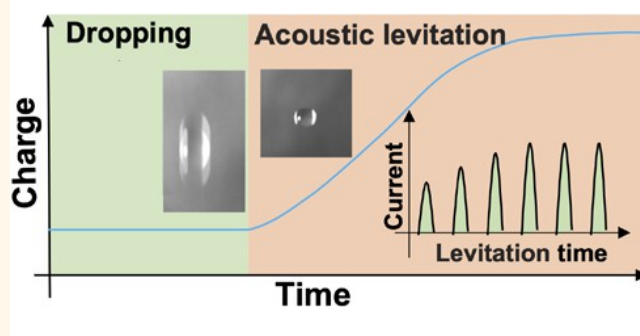
Article Recommendations



Supporting Information

ABSTRACT: It is known that the suspended liquid droplets in clouds can generate electrostatic charges, which finally results in the lightning. However, the detailed mechanism related to the contact-electrification process on the liquid-gas (L-G) interfaces is still poorly understood. Here, by introducing an acoustic levitation method for levitating a liquid droplet, we have studied the electrification mechanism at the L-G interface. The tribo-motion between water droplets and air induced by the ultrasound wave leads to the generation of positive charges on the surface of the droplets, and the charge amount of water droplets (20 μL) gradually reaches saturation within 30 s. The mixed solid particles in droplets can increase the amount of transferred charge, whereas the increase of ion concentration in the droplet can suppress the charge generation. This charge transfer phenomenon at L-G interfaces and the related analysis can be a guidance for the study in many fields, including anti-static, harvesting rainy energy, micro/nano fluidics, triboelectric power generator, surface engineering, and so on. Moreover, the surface charge generation due to L-G electrification is an inevitable effect during ultrasonic levitation, and thus, this study can also work for the applications of the ultrasonic technique.

KEYWORDS: contact electrification, charge transfer, liquid-gas interfaces, solid-gas interfaces, nanogenerator



The phenomenon of surface electrification upon contact has been documented for over 2600 years, and many applications have been developed based on this phenomenon.^{1–4} Since 2012, the triboelectric nanogenerator (TENG) proposed by Wang, which uses the coupling of contact electrification and electrostatic induction to generate electrical energy, has been a further understanding of the mechanism of frictional power and gradually developing as one technology in the field of energy harvesting.^{5–9} The operation of a TENG mainly relies on the interfacial electrostatic field, which outputs power due to the displacement current induced by mechanical motion.^{10–13} So far, TENGs can harvest energy from tribo-contacts at the solid-solid interface,^{14–17} solid-liquid interface,^{18–22} liquid-liquid interface,^{23,24} and even solid-gas interface,²⁵ while the applications of TENGs have also been successfully developed in many areas, including micro/nano power source,^{26–28} self-powered sensors,^{29–32} blue energy harvester,^{33–36} and high-voltage sources.^{37–39} However, little progress has been proposed related to energy generation at the liquid-gas (L-G) interface. It is commonly known that lightning on rainy days and lightning of dressing coats are the results of triboelectricity, which can be an undeveloped energy source. However, the lack of knowledge on mechanisms for electrostatic

charge accumulation and dissipation on an L-G interface also prevents the collection and use of energy from the atmospheric electricity. During the contact motion between liquid and gas, it is not easy to realize sufficient tribo-motion due to the low density of the gas and low moving velocity of the liquid. Hence, the liquid-gas interface remains undeveloped for researchers in the field of TENG.

On the other hand, the acoustic levitation technique is a kind of noncontact manipulation method using acoustic radiation force exerted by sound waves to levitate almost any kind of material in a smaller space, including solids, liquids, and even small living animals.^{40–48} Acoustic levitation is not only an interesting physical phenomenon but also a promising tool for multiple disciplines such as biology, chemistry, or pharmacy.^{49–52} The special features of acoustic levitation also have

Received: August 18, 2021

Accepted: October 18, 2021

great potential for performing some tasks in industry such as the contactless manipulation of fragile objects or processing small volumes of liquids, while it can also be employed for trapping, sorting, and manipulating microparticles and cells inside a liquid medium.^{53–55} In this case, the acoustic levitation technique can possibly maintain highly controllable tribo-motion between droplet and air.

In this work, we clarified the charge transfer process between liquid droplets and air. The stable L-G interface can be achieved by introducing a low power and portable acoustic levitation device for suspending liquid drops in different gas. The levitated liquid droplets rotate at a very high speed in the acoustic wave, leading to a stable and fast tribo-motion between liquid droplet and gas. The charge amount on the levitated droplets increases with the increase of levitating time, while the charge amount finally reaches saturation state with the extension of the suspension time. Different suspensions and ionic liquids are used for contacting with air, while ions accumulating on the L-G interface can create a screen effect to suppress the charge generation on the L-G interface. Furthermore, charge generation on L-G interfaces is significantly enhanced in the air near an electrified object, indicating that charges on the solid surface can escape into air and the air molecule carrying charges can influence the electrification process on L-G interfaces. The experimental system and the related physical analysis can be of help to the study of rainy energy harvesting, micro/nano fluidics, triboelectric power generator, surface engineering, and so on. Moreover, this study shows that the contact-electrification at L-G interfaces induced by the ultrasonic vibration/rotation is a notable effect, which should be further considered for various ultrasonic manipulation systems.

RESULTS/DISCUSSION

As shown in Figure 1A, the raindrop usually carries some electrostatic charges due to the tribo-motion with air. However, the underlying mechanism related to the charge generation process on this L-G interface is still not fully clarified. With the increase of the falling height of the droplets, the relative motion between droplet and air is enhanced, and accordingly, the static charges gradually accumulate on the surface of the water droplets. However, in order to achieve enough relative motion between water droplets and gas, a falling height of at least a hundred meters is required, which is difficult to be achieved based on common experimental equipment. In this study, the acoustic field is used for suspending liquid drops, which is generated by two ultrasonic phased arrays (see Figure 1B and Supplementary Figure 1). The focal point of the sound is formed by precisely tuning the sound wave frequency to 40 kHz, while a Faraday cup is placed underneath the levitated droplet (see Figure 1C). A precision stepping motor is used to push the needle tube, in order to put the droplet with precisely controlled volume at the focal point of the acoustic field (the volume of each drop is 20 μL). The droplet rotates at a very high speed in the acoustic field, while a high-speed camera is used to measure the radius, elevation, and state of droplets from the side view. An ultrasensitive electrometer equipped with a Faraday cup made of an aluminum sheet to shield external interference is used to quantify the electrification of the water droplet. Electrical charges on levitated droplets are measured by integrating the induced short-circuit current from the Faraday cup when the droplet is dripping into the Faraday cup. The dynamic behaviors of the levitated droplet found at the stable suspension stage are studied by using a high-speed camera, as shown in Figure 1D. It

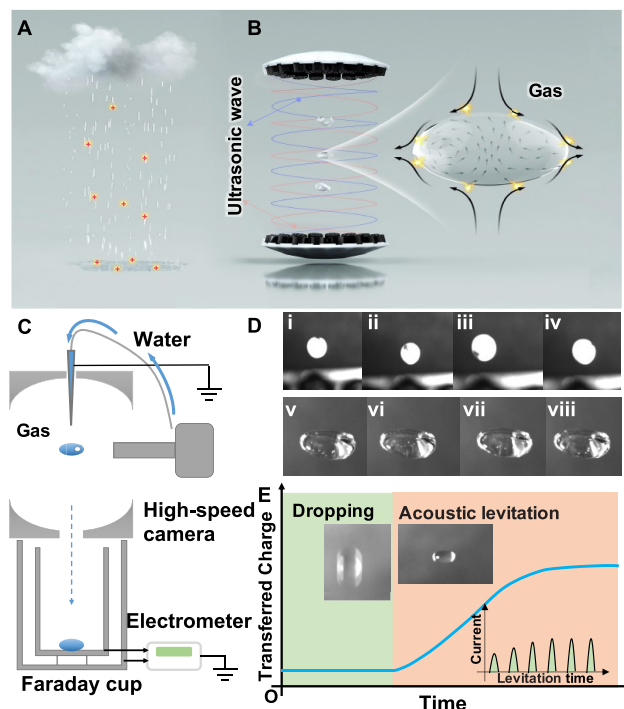


Figure 1. Phenomena of liquid-gas contact electrification and schematics of the experimental setups. (A) Contact electrification between falling raindrops and air in nature. (B) Contact electrification between water droplets and gas in an ultrasonic suspension device. (C) Direct measurement of electrical charges carried by water droplets using a Faraday cup (comprising an aluminum sheet) connected to an electrometer. (D) (i–iv) A foam ball rotating at high speed (a black spot on the surface of the foam ball as a reference point); (v–viii) internal flow observation of PS microspheres in the levitated water drop. (E) Transferred charge from air to levitated water droplet increases with suspension time and finally tends to saturation.

has been found that the levitated droplet can stably rotate at a speed of 7200 rpm, resulting in a sufficient tribo-motion with air (see Figure 1D (i–iv) and Movie S1). The detailed rotation mode of the droplet can be seen in Figure 1B,D, which allows the internal part of the droplet to move to the outside and the complete contact between liquids and air can be achieved (see Figure 1D (v–viii) and Movie S2).

In this study, the high-speed rotation of the suspended liquid droplets in the acoustic field can provide sufficient tribo-motion between water molecules and gas molecules, leading to the high probability of contact electrification. We have done our best to clean the air and remove the floating charges, as explained in the Experimental Section. The charge amount on the droplet is increased with the increase of suspension time, while the droplet is fixed at the same position and there is no significant air flow in the chamber. Hence, we believed that the charge separation between liquid and gas is the main origin of this electrification process. To better understand the mechanism of tribo-electrification at L-G interfaces, the similar theory of intermolecular electron clouds is employed, as shown in Supplementary Figure 1. The liquid droplets suspended by ultrasonic contain more charges than the droplets with direct falling, while the charge of the droplets tends to be saturated with the extension of the suspension time (see in Figure 1E). Small-scale objects, including liquid drops, gas bubbles, solid

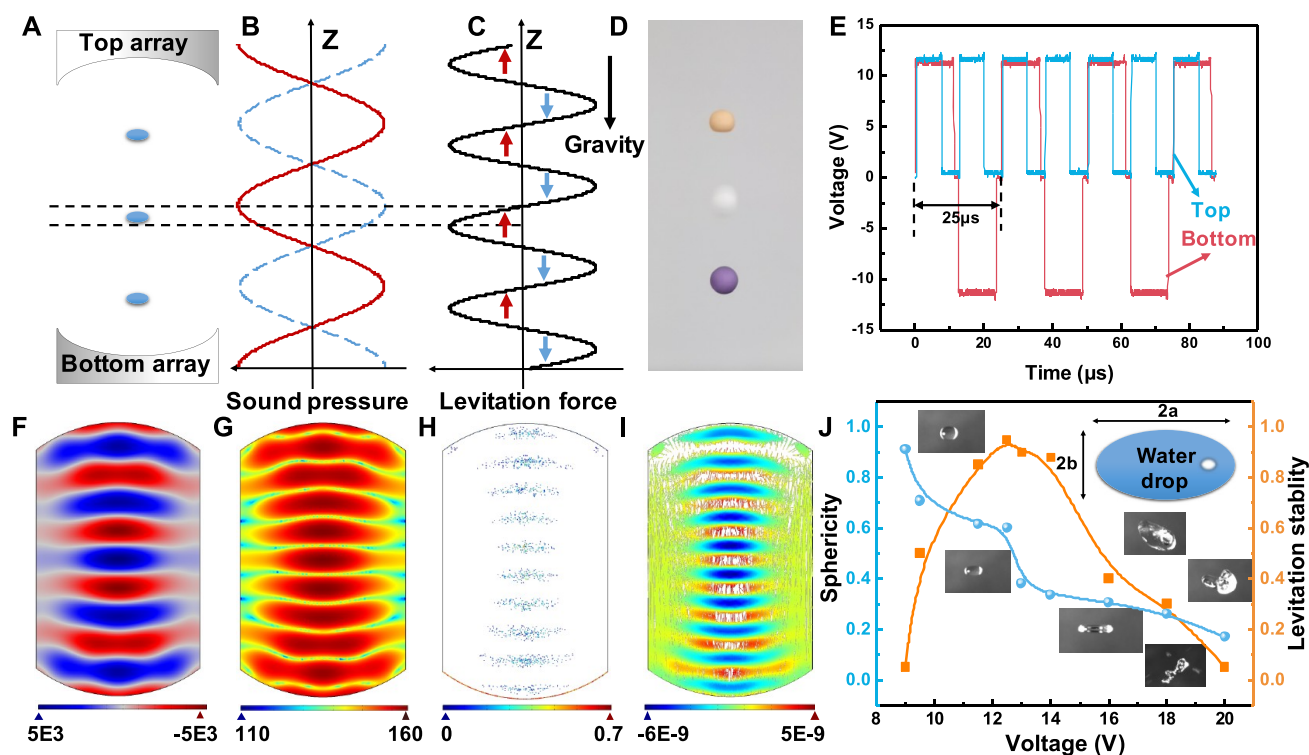


Figure 2. Working principles of acoustic levitation. (A) Structure of the acoustic levitation. (B) Sound pressure and (C) radiation force in acoustic levitation standing wave field. (D) Three foam spheres are suspended in midair. (E) Excitation drive voltage applied to the ultrasonic system for controlling the position of the droplet in the chamber, either at the top or at the bottom. (F) Pressure amplitude distribution. (G) Sound pressure levels in the levitator. (H) Positions of the particles at $t = 0.1$ s. The colors refer to the instantaneous particle velocities. (I) Particle position and trajectories plotted using the radiation potential as coloring. (J) Plot of the levitated droplet's sphericity and stability as a function of applied voltage.

particles, *etc.*, in a gas fluid can experience a stable time-averaged force when irradiated by a sound field, which is referred to as acoustic radiation force. Gor'kov developed a general theory based on the acoustic force potential U_{ac} suitable to compressible particles, which can be written as^{56,57}

$$U_{ac} = \frac{4\pi}{3} r^3 \left[f_1 \frac{1}{2\rho_M C_M^2} \langle p^2 \rangle - f_2 \frac{3}{4} \rho_M \langle v^2 \rangle \right] \quad (1)$$

$$f_1 = 1 - \frac{k_p}{k_M} \quad (2)$$

$$f_2 = \frac{2(\rho_p - \rho_M)}{(2\rho_p + \rho_M)} \quad (3)$$

For the acoustic levitation in air, the potential U_{ac} can be simplified as

$$U_{ac} = 2\pi r^3 \left[\frac{\langle p^2 \rangle}{3\rho_0 C_0} - \frac{p \langle v^2 \rangle}{2} \right] \quad (4)$$

where ρ_0 is the density of air and c_0 is the sound velocity in air. The acoustic levitator consists of two ultrasonic transmitter arrays, as illustrated in Figure 2A–C and Supplementary Figure 2. The samples, either solid or liquid, can be levitated at the pressure nodes of the sound field, each of which is separated by a distance of $\lambda/2$. For the levitation of a liquid droplet, the goal is not simply to balance gravity. A force balance at the droplet

surface must be obtained. The acoustic radiation pressure on the droplet is not uniform, usually positive (compression) at the polar area, while negative (suction) at the equator, as illustrated in Supplementary Figure 3. The droplet will, in turn, adjust its surface curvature to adapt the radiation pressure. Meanwhile, the Bernoulli effect arising from the acoustic streaming may alter the force balance on the levitated sample and bring additional instability. To enhance the levitation ability and stability, both ultrasonic transmitter arrays are often made concave. In order to make the droplet suspend stably, two different kinds of nonarray ultrasonic levitation devices are also designed as shown in Supplementary Figures 4 and 5. Finally, the double array ultrasonic levitation device with higher stability and suspension capacity is selected as the experimental system. To show the position of the standing point and its stability of levitation, we put foam balls on the central axis, where the foam ball can be suspended (see in Figure 2D).

As shown in Supplementary Figure 6, the ultrasonic suspension system consists of two ultrasonic transmitter arrays, a driver (L298N), controller (Arduino Nano), and computer. The Arduino Nano programmed by the computer generates the square wave signals to control the L298N Dual H-Bridge motor driver for amplifying the signals to power the ultrasonic transmitter arrays. One channel is kept at a constant phase, while the other channel's phase can be shifted to move the trapped particles upward or downward. The cycle time of the driving voltage signal is $25 \mu\text{s}$, so the final ultrasonic frequency is about 40 MHz, as shown in Figure 2E. To understand the

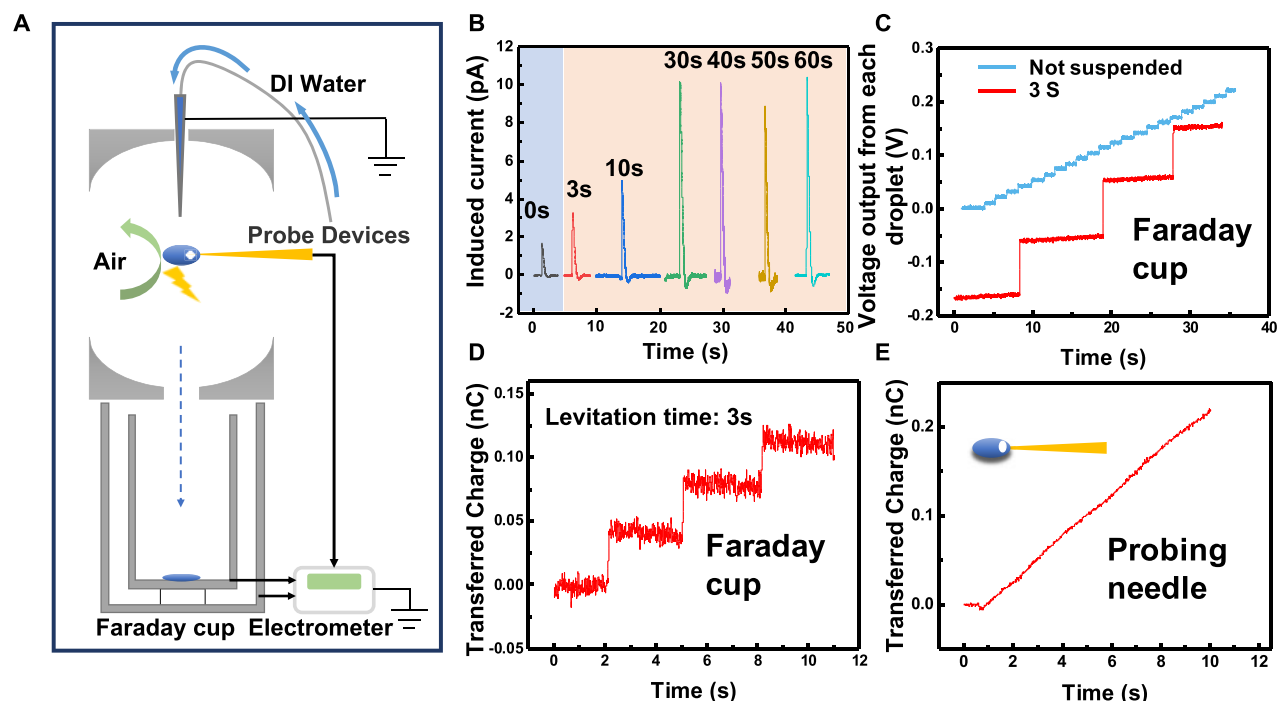


Figure 3. Contact electrification between levitated DI water droplets and air. (A) Schematic showing experimental setup. Experimental setup is placed in a Faraday cage. (B) Induced current signals from Faraday cup after tribo-motion between DI water droplets and air in different suspension time. (C) Voltage output of levitated droplets (from Faraday cup) with a suspension time of 3 s (see the red curve). The blue curve is the voltage output of water droplets without acoustic levitation. (D) Transferred charge of levitated droplets (from Faraday cup) with a suspension time of 3 s. (E) The transferred charge when probing needle is inserted into suspended DI water droplets.

physical mechanism of acoustic levitation, we use the COMSOL software to numerically calculate the pressure amplitude and the sound pressure field between two ultrasonic transmitter arrays. The pressure field is shown in Figure 2F, with plane wave radiation conditions at the open boundaries. The corresponding sound pressure level in the system is shown in Figure 2G. This distribution strongly depends on the ultrasonic transmitter array geometry which plays an essential role in enhancing levitation ability and stability. Meanwhile, the position of the particles at $t = 0.1$ s is shown in Figure 2H and Movie S3. Finally, the particle position and its trajectories are shown in Figure 2I using the magnitude of the radiation potential as a color legend. Since the radiation force is defined as the gradient of the radiation potential, it is clear that the particles tend toward the lowest potential value.

In addition to numerous structure parameters of the system, the voltage of the transducer also has a significant effect on the shape and stability of droplets within acoustic levitation systems (see in Supplementary Figure 7). The data in Figure 2J show the relationship between droplet sphericity (as determined using eq 5 in Experimental Section) and spatial stability (as determined using eq 6 in Experimental Section), as a function of the applied voltage for the levitating system. It is found that there is a decline in the droplet sphericity as a function of applied voltage which remained above 60% until 12.5 V. The stability, however, reaches the maximum value at 12.5 V. This suggests that 12.5 V represented the best option to maintain both drop stability and sphericity for these samples, and this voltage is used for all the related experiments.

To understand electrification at L-G interfaces, the ultrasonic suspension device and the Faraday cup are combined to avoid external interference of static electricity (see in Figure 3A and

Supplementary Figure 7). After the levitation, the droplet with different surface charges falls into the Faraday cup. The size of each water droplet is precisely controlled by the stepping motor, and the long metal needle is grounded to avoid the ambient influences. Usually, the increase in ion concentration in a liquid is a negative effect for electrification, which can be attributed to the screen effect due to the existence of H^+ and OH^- in water. Hence, the deionized water (DI water) is used as the liquid contact pairs to amplify the electrification results. As shown in Figure 3B, the peak value of the output current increases after the water droplet levitated in different times. Here, the output signal is measured from the Faraday cup, where the dripping of the droplet into the cup can induce the output signal from the cup to the ground. When the suspension time of water droplets is more than 30 s, the peak value of the current reaches a maximum value, suggesting that the electrification process between water droplets and air reaches saturation. In order to prove the effects of ultrasound on contact electrification at the L-G interface, we conduct a comparative experiment without ultrasound. As shown in Figure 3C, each droplet without ultrasonic suspension can induce a voltage output (from Faraday cup) for about 0.014 V, and the same signal after ultrasonic suspension (3 s) is 0.11 V. The charge amount of water droplets with a suspension time of 3 s is shown in Figure 3D, and the charge carried by each droplet is about 0.05 nC. At the same time, in order to measure the real-time charge on suspended water droplets, the probe is used to insert into the water droplets, and then, the electrical signal of the probe is measured with the 6514 electrometer. As shown in Figure 3E, the charge increase rate of the levitated water droplet is about 25 pC/s, and the transferred charge curve shows an increasing trend without saturation, since the electric charge accumulated by contact

electrification at the L-G interface is transferred to the instrument.

To further explore the contact electrification between water droplets and different gases, we design a closed acoustic levitation chamber filled with O₂, N₂, and Ar, respectively, to make the suspended water droplets fully contact with gas (see in Figure 4A). The sound absorption sponge is put on the inner

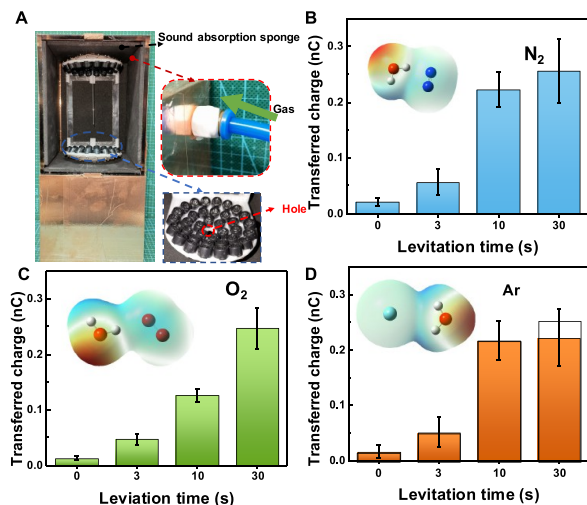


Figure 4. Contact electrification between levitated water droplets and different kinds of gases. (A) Photograph of sealed acoustic levitation equipment with two ultrasonic emitter arrays. A hole is in the middle of the bottom array in order to let the water drop into the Faraday cup. The transferred charge (from Faraday cup) of the DI water droplet with different levitation time (B) in a N₂ atmosphere, (C) in an O₂ atmosphere, and (D) in an Ar atmosphere.

wall to prevent the reflection of ultrasonic waves on the inner wall from causing water droplets instability and bursting. As

shown in Figure 4B–D, with the extension of suspension time, the output transferred charge from the Faraday cup also increases, which shows that transfer charge exists with different gas. As can be seen from Figure 4B–D, the charge transferred by tribo-motion between suspended water droplets with Ar (suspension time: 30 s) is less than that with O₂ and N₂. The detailed reason related to this point may still need further study. To further explore the effect of charge transfer at the L-G interface, different mixed liquids and ionic liquids are used for the following experiments (see in Figure 5A–D). PTFE suspension and BaTiO₃ suspension are chosen to be levitated in the midair. The transferred charges of PTFE and BaTiO₃ suspension droplets are opposite to that of the DI water droplet (see in Figure 5A,B), while the transferred charges of Nylon suspension droplets and NaCl solution are both positive (see in Figure 5C,D). As shown in Figure 5D, the transferred charge of NaCl solution droplets remains nearly unchanged in different water droplet suspension time since the presence of freely moving ions in the NaCl ion solution forms an electrostatic shielding effect. From Figure 5A–C, the results show that the absolute value of transferred charge of the suspensions of PTFE, BaTiO₃ is obviously greater than that of DI water, which suggests that there is contact electrification between suspended particles and air at solid-gas interfaces, as shown in Supplementary Figure 9.

Meanwhile, we also explore the effect of external electrostatic field on the contact electrification on L-G interfaces. The Polyimide film and Nylon film are rubbed against each other in advance, and then they were made as rings, where the surface charge densities of these two films are 90 and 76 $\mu\text{C}/\text{m}^2$, respectively. These rings with a strong electrostatic field are placed on the central axis of the ultrasonic suspension, and the suspended DI water droplet is suspended in the center of the ring, as shown in Figure 5E. When the DI water droplet is levitated in the center of the Polyimide ring, the transferred charge from the Faraday cup after its falling is opposite with that

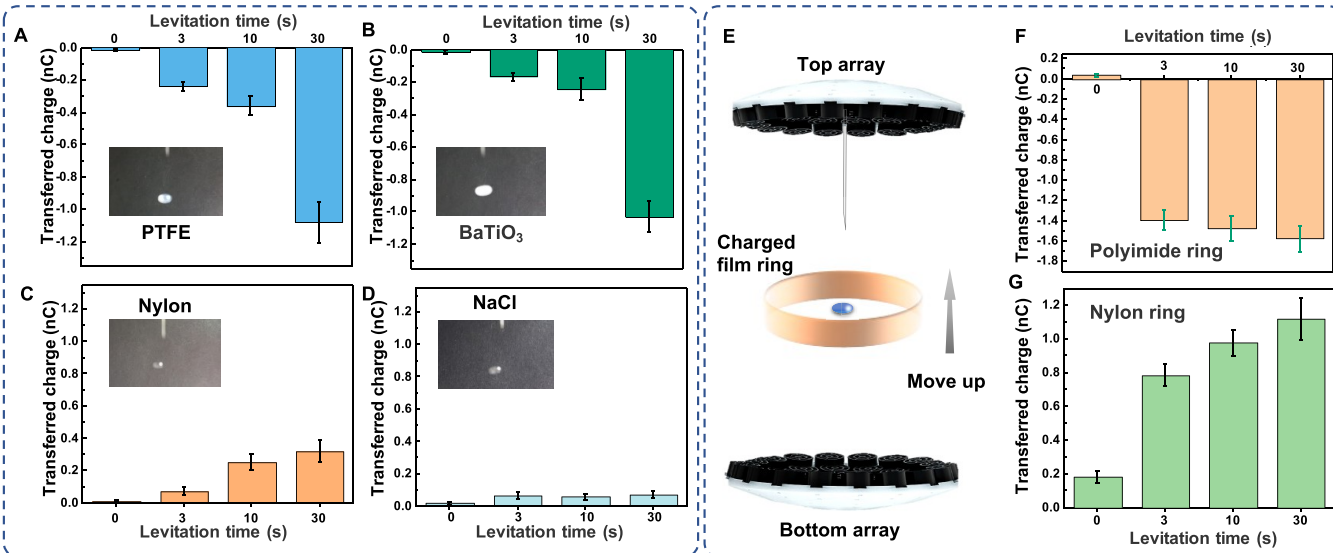


Figure 5. Contact electrification between levitated different liquid droplets and air, and the effect of the electrostatic field polarization ring on levitated DI water droplets. (A) Measured amount of transferred charge (from Faraday cup) of PTFE suspension droplets in air in different levitation time. The transferred charge (from Faraday cup) of (B) BaTiO₃ suspension droplets, (C) Nylon suspension droplets, and (D) NaCl solution droplets. (E) Diagram of the experimental setup. The DI water droplet is levitated in the center of a charged film ring. (F) The transferred charge (from Faraday cup) of water droplets levitated in the center of Polyimide film ring. (G) The transferred charge of water droplets levitated in the center of Nylon film ring.

of naturally falling water droplets (without external field; see [Supplementary Figure 10](#)), and the absolute value of the transferred charge is much larger (see in [Figure 5F](#)). The negative charges are induced on the surface of the Polyimide ring due to the contact electrification, while the charge relaxation for the surface to the air allows the surrounding air carrying negative charges. The levitated DI water droplets are rotating at a high speed tribo-motion with the surrounding air, and the negative charges are transferred to the droplet, as shown in [Supplementary Figure 11](#). The direction of its transferred charge is the same as that of naturally falling water droplets as the DI water droplet suspended in the center of the Nylon ring (positively charged) (see in [Figure 5G](#)). Hence, these results confirm that the electrification on the L-G interface is easily influenced by the surroundings, and a well-controlled experimental environment is inevitable for clarifying the underlying mechanism of L-G electrification.

CONCLUSIONS

In summary, we have investigated the mechanism of L-G contact electrification supported by using a low cost, low power, and portable acoustic levitator to suspend liquid droplets in the related air. The liquid droplets rotate at a very high speed in the acoustic field, which provides a stable experimental condition to support sufficient tribo-contact between droplet and air. Hence, contact electrification at L-G interfaces can be verified without much concern about liquid vaporization. In this work, we get the following interrelated conclusions:

- (i) Friction between levitated DI water droplets and air (temperature: 25 °C, relative humidity: 21%) makes DI droplets carry a positive charge.
- (ii) We observed that the charge amount of water droplets (20 μL) gradually becomes saturated with the levitation time of 30 s.
- (iii) Different suspended particles (PTFE, BaTiO₃, Nylon) in DI water droplets can increase the amount of charge transfer, whereas ionic solution (NaCl solution, 0.1 mol/L) has a suppression effect on charge transfer due to the screen effect.
- (iv) The transfer of charge amount at L-G interfaces can be significantly enhanced, if the droplet is levitated in the air near a strongly charged solid surface, indicating that the charge transfer process from solid to air and then to droplet is possible.

These findings advance the scientific understanding of contact electrification at L-G interfaces and guide reasonable design technologies including anti-static, micro/nano fluidics, triboelectric power generator, and materials and surface engineering. Moreover, since the contact electrification at L-G interfaces induced by the ultrasonic vibration/rotation is inevitable, the study in this work can also help to further optimize various ultrasonic manipulation systems.

METHODS/EXPERIMENTAL SECTION

Sample Preparation. The DI water with a resistivity of 18.2 M Ω -cm used here was produced by a deionizer (HHitech, China). Before the experiments, the Faraday cup was cleaned with alcohol and DI water and heated for 10 min at 350 K to remove the charge on the surfaces. During the contact electrification between water droplets and air, the ultra-clean air is used to pass into the closed experimental environment, and then stand for 30 min. In the contact electrification between water droplets and other gases (N₂, O₂, Ar, respectively), the gas is pumped

into the closed experimental environment for 30 min; then ultrasonic levitation and charge measurement are performed.

Calculation of Sphericity of the Levitated Liquid Droplets.

There is a trade-off between higher voltages which ensure stable entrapment (up to the point at which the droplets are split into smaller volumes) at the expense of maintaining sphericity and providing sufficient acoustic pressure to levitate their mass. We present a combined plot of sphericity and stability for a silicone oil coated water droplet to determine the optimum range of voltages suitable for such an experiment

$$\psi = \frac{2\sqrt[3]{ab^2}}{a + \frac{b^2}{\sqrt{a^2-b^2}} \ln\left(\frac{a + \sqrt{a^2-b^2}}{b}\right)} \quad (5)$$

where a and b are the semi-major and semi-minor axes, respectively, as determined from the ellipse fitting function.

Calculation of Stability of the Levitated Liquid Droplets.

Twenty drops of DI water droplets (20 μL) are placed in the same ultrasonic standing point and suspended for 60 s; then the proportion of water droplets that can be stably suspended is calculated, which is assumed to be the magnitude of stability (\emptyset).

$$\emptyset = \frac{N_s}{20} \quad (6)$$

where N_s is the number of water droplets that can be stably suspended.

ASSOCIATED CONTENT

Supporting Information

The Supporting Information is available free of charge at <https://pubs.acs.org/doi/10.1021/acsnano.1c07158>.

Supplementary Figures 1–11 show the mechanism of contact electrification, the structure of ultrasonic levitation system, the experimental setup images, and electrical output performance of contact electrification at L-G interface ([PDF](#))

Movie S1 shows that the levitated droplet can stably rotate at a high speed, resulting in a sufficient tribo-motion with air ([AVI](#))

Movie S2 shows motivation of the internal particles of the droplet ([AVI](#))

Movie S3 shows motivation simulation of particles in ultrasonic suspension system ([AVI](#))

AUTHOR INFORMATION

Corresponding Authors

Xiangyu Chen – CAS Center for Excellence in Nanoscience, Beijing Key Laboratory of Micro-nano Energy and Sensor, Beijing Institute of Nanoenergy and Nanosystems, Chinese Academy of Sciences, Beijing 100083, China; School of Nanoscience and Technology, University of Chinese Academy of Sciences, Beijing 100049, China; orcid.org/0000-0002-0711-0275; Email: chenxiangyu@binn.cas.cn

Zhong Lin Wang – CAS Center for Excellence in Nanoscience, Beijing Key Laboratory of Micro-nano Energy and Sensor, Beijing Institute of Nanoenergy and Nanosystems, Chinese Academy of Sciences, Beijing 100083, China; School of Nanoscience and Technology, University of Chinese Academy of Sciences, Beijing 100049, China; School of Material Science and Engineering, Georgia Institute of Technology, Atlanta, Georgia 30332-0245, United States; orcid.org/0000-0002-5530-0380; Email: zhong.wang@mse.gatech.edu

Authors

Fan Wang – CAS Center for Excellence in Nanoscience, Beijing Key Laboratory of Micro-nano Energy and Sensor, Beijing Institute of Nanoenergy and Nanosystems, Chinese Academy of Sciences, Beijing 100083, China; School of Nanoscience and Technology, University of Chinese Academy of Sciences, Beijing 100049, China

Peng Yang – CAS Center for Excellence in Nanoscience, Beijing Key Laboratory of Micro-nano Energy and Sensor, Beijing Institute of Nanoenergy and Nanosystems, Chinese Academy of Sciences, Beijing 100083, China; School of Nanoscience and Technology, University of Chinese Academy of Sciences, Beijing 100049, China

Xinglin Tao – CAS Center for Excellence in Nanoscience, Beijing Key Laboratory of Micro-nano Energy and Sensor, Beijing Institute of Nanoenergy and Nanosystems, Chinese Academy of Sciences, Beijing 100083, China; School of Nanoscience and Technology, University of Chinese Academy of Sciences, Beijing 100049, China

Yuxiang Shi – CAS Center for Excellence in Nanoscience, Beijing Key Laboratory of Micro-nano Energy and Sensor, Beijing Institute of Nanoenergy and Nanosystems, Chinese Academy of Sciences, Beijing 100083, China; School of Nanoscience and Technology, University of Chinese Academy of Sciences, Beijing 100049, China; orcid.org/0000-0001-5112-4159

Shuyao Li – CAS Center for Excellence in Nanoscience, Beijing Key Laboratory of Micro-nano Energy and Sensor, Beijing Institute of Nanoenergy and Nanosystems, Chinese Academy of Sciences, Beijing 100083, China; School of Nanoscience and Technology, University of Chinese Academy of Sciences, Beijing 100049, China; orcid.org/0000-0003-2156-4684

Zhaoqi Liu – CAS Center for Excellence in Nanoscience, Beijing Key Laboratory of Micro-nano Energy and Sensor, Beijing Institute of Nanoenergy and Nanosystems, Chinese Academy of Sciences, Beijing 100083, China; School of Nanoscience and Technology, University of Chinese Academy of Sciences, Beijing 100049, China

Complete contact information is available at: <https://pubs.acs.org/10.1021/acsnano.1c07158>

Author Contributions

X.C. and Z.L.W. conceived the idea and supervised the experiment. F.W. prepared the manuscript. F.W. and P.Y. designed the structure of the device. F.W. performed the data measurements. S.L. and Z.L. offered assistance with the experiments. All the authors discussed the results and commented on the manuscript.

Notes

The authors declare no competing financial interest.

ACKNOWLEDGMENTS

This work was supported by the National Natural Science Foundation of China (Grant No. 51775049), the Beijing Natural Science Foundation (4192069), the Beijing Municipal Science & Technology Commission (Z171100000317001), and the Young Top-Notch Talents Program of Beijing Excellent Talents Funding (2017000021223ZK03), Beijing Nova program (Z201100006820063), and Youth Innovation Promotion Association CAS (20211165).

REFERENCES

- (1) Wang, Z. L.; Wang, A. C. On the Origin of Contact-Electrification. *Mater. Today* **2019**, *30*, 34–51.
- (2) Lin, S.; Chen, X.; Wang, Z. L. Contact Electrification at the Liquid–Solid Interface. *Chem. Rev.* **2021**, DOI: [10.1021/acs.chemrev.1c00176](https://doi.org/10.1021/acs.chemrev.1c00176).
- (3) Gibson, H. W. Linear Free Energy Relations. V. Triboelectric Charging of Organic Solids. *J. Am. Chem. Soc.* **1975**, *97* (13), 3832–3833.
- (4) Vácha, R.; Marsalek, O.; Willard, A. P.; Bonthuis, D. J.; Netz, R. R.; Jungwirth, P. Charge Transfer between Water Molecules as the Possible Origin of the Observed Charging at the Surface of Pure Water. *J. Phys. Chem. Lett.* **2012**, *3* (1), 107–111.
- (5) Zhang, Q.; Jiang, C.; Li, X.; Dai, S.; Ying, Y.; Ping, J. Highly Efficient Raindrop Energy-Based Triboelectric Nanogenerator for Self-Powered Intelligent Greenhouse. *ACS Nano* **2021**, *15* (7), 12314–12323.
- (6) Xu, W.; Zheng, H.; Liu, Y.; Zhou, X.; Zhang, C.; Song, Y.; Deng, X.; Leung, M.; Yang, Z.; Xu, R. X.; Wang, Z. L.; Zeng, X. C.; Wang, Z. A Droplet-Based Electricity Generator with High Instantaneous Power Density. *Nature* **2020**, *578* (7795), 392–396.
- (7) Li, S.; Nie, J.; Shi, Y.; Tao, X.; Wang, F.; Tian, J.; Lin, S.; Chen, X.; Wang, Z. L. Contributions of Different Functional Groups to Contact Electrification of Polymers. *Adv. Mater.* **2020**, *32* (25), 2001307.
- (8) Wang, F.; Ren, Z.; Nie, J.; Tian, J.; Ding, Y.; Chen, X. Self-Powered Sensor Based on Bionic Antennae Arrays and Triboelectric Nanogenerator for Identifying Noncontact Motions. *Adv. Mater. Technol.* **2020**, *5* (1), 1900789.
- (9) Shi, Y.; Wang, F.; Tian, J.; Li, S.; Fu, E.; Nie, J.; Lei, R.; Ding, Y.; Chen, X.; Wang, Z. L. Self-Powered Electro-Tactile System for Virtual Tactile Experiences. *Sci. Adv.* **2021**, *7* (6), No. eabe2943.
- (10) Li, S.; Fan, Y.; Chen, H.; Nie, J.; Liang, Y.; Tao, X.; Zhang, J.; Chen, X.; Fu, E.; Wang, Z. L. Manipulating the Triboelectric Surface Charge Density of Polymers by Low-Energy Helium Ion Irradiation/Implantation. *Energy Environ. Sci.* **2020**, *13* (3), 896–907.
- (11) Zhang, H.; Yang, Y.; Su, Y.; Chen, J.; Hu, C.; Wu, Z.; Liu, Y.; Ping Wong, C.; Bando, Y.; Wang, Z. L. Triboelectric Nanogenerator as Self-Powered Active Sensors for Detecting Liquid/Gaseous Water/Ethanol. *Nano Energy* **2013**, *2* (5), 693–701.
- (12) Lin, Z.; Zhang, B.; Guo, H.; Wu, Z.; Zou, H.; Yang, J.; Wang, Z. L. Super-Robust and Frequency-Multiplied Triboelectric Nanogenerator for Efficient Harvesting Water and Wind Energy. *Nano Energy* **2019**, *64*, 103908.
- (13) Xu, M.; Wang, S.; Zhang, S. L.; Ding, W.; Kien, P. T.; Wang, C.; Li, Z.; Pan, X.; Wang, Z. L. A Highly-Sensitive Wave Sensor Based on Liquid-Solid Interfacing Triboelectric Nanogenerator for Smart Marine Equipment. *Nano Energy* **2019**, *57*, 574–580.
- (14) Bai, P.; Bazant, M. Z. Charge Transfer Kinetics at the Solid–Solid Interface in Porous Electrodes. *Nat. Commun.* **2014**, *5* (1), 3585.
- (15) Tu, Z.; Choudhury, S.; Zachman, M. J.; Wei, S.; Zhang, K.; Kourkoutis, L. F.; Archer, L. A. Fast Ion Transport at Solid–Solid Interfaces in Hybrid Battery Anodes. *Nature Energy* **2018**, *3* (4), 310–316.
- (16) A Correspondent. Solid-Solid Interfaces. *Nature* **1968**, *218* (5137), 117..
- (17) Li, X.; Jiang, C.; Ying, Y.; Ping, J. Biotriboelectric Nanogenerators: Materials, Structures, and Applications. *Adv. Energy Mater.* **2020**, *10* (44), 2002001.
- (18) Lin, S.; Xu, L.; Chi Wang, A.; Wang, Z. L. Quantifying Electron-Transfer in Liquid-Solid Contact Electrification and the Formation of Electric Double-Layer. *Nat. Commun.* **2020**, *11* (1), 399.
- (19) Lin, S.; Zheng, M.; Wang, Z. L. Detecting the Liquid–Solid Contact Electrification Charges in a Liquid Environment. *J. Phys. Chem. C* **2021**, *125* (25), 14098–14104.
- (20) Nie, J.; Ren, Z.; Xu, L.; Lin, S.; Zhan, F.; Chen, X.; Wang, Z. L. Probing Contact-Electrification-Induced Electron and Ion Transfers at a Liquid – Solid Interface. *Adv. Mater.* **2020**, *32* (2), 1905696.
- (21) Choi, D.; Lee, D.; Sung Kim, D. A Simple Approach to Characterize Gas-Aqueous Liquid Two-Phase Flow Configuration

- Based on Discrete Solid-Liquid Contact Electrification. *Sci. Rep.* **2015**, *5* (1), 15172.
- (22) Nauruzbayeva, J.; Sun, Z.; Gallo, A.; Ibrahim, M.; Santamarina, J. C.; Mishra, H. Electrification at Water–Hydrophobe Interfaces. *Nat. Commun.* **2020**, *11* (1), 5285.
- (23) Zhao, X.; Lu, X.; Zheng, Q.; Fang, L.; Zheng, L.; Chen, X.; Wang, Z. L. Studying of Contact Electrification and Electron Transfer at Liquid-Liquid Interface. *Nano Energy* **2021**, *87*, 106191.
- (24) Nie, J.; Wang, Z.; Ren, Z.; Li, S.; Chen, X.; Lin Wang, Z. Power Generation from the Interaction of a Liquid Droplet and a Liquid Membrane. *Nat. Commun.* **2019**, *10* (1), 2264.
- (25) Xiong, J.; Thangavel, G.; Wang, J.; Zhou, X.; Lee, P. S. Self-Healable Sticky Porous Elastomer for Gas-Solid Interacted Power Generation. *Sci. Adv.* **2020**, *6* (29), No. eabb4246.
- (26) Zhong, W.; Xu, L.; Zhan, F.; Wang, H.; Wang, F.; Wang, Z. L. Dripping Channel Based Liquid Triboelectric Nanogenerators for Energy Harvesting and Sensing. *ACS Nano* **2020**, *14* (8), 10510–10517.
- (27) Kaponig, M.; Mölleken, A.; Nienhaus, H.; Möller, R. Dynamics of Contact Electrification. *Sci. Adv.* **2021**, *7* (22), No. eabg7595.
- (28) Jiang, C.; Li, X.; Ying, Y.; Ping, J. A Multifunctional TENG Yarn Integrated into Agrotexile for Building Intelligent Agriculture. *Nano Energy* **2020**, *74*, 104863.
- (29) Huang, J.; Yang, X.; Yu, J.; Han, J.; Jia, C.; Ding, M.; Sun, J.; Cao, X.; Sun, Q.; Wang, Z. L. A Universal and Arbitrary Tactile Interactive System Based on Self-Powered Optical Communication. *Nano Energy* **2020**, *69*, 104419.
- (30) Ding, Y.; Shi, Y.; Nie, J.; Ren, Z.; Li, S.; Wang, F.; Tian, J.; Chen, X.; Wang, Z. L. Thermochromic Triboelectric Nanogenerator Enabling Direct Visualization of Temperature Change during Operation. *Chem. Eng. J.* **2020**, *388*, 124369.
- (31) Ren, Z.; Ding, Y.; Nie, J.; Wang, F.; Xu, L.; Lin, S.; Chen, X.; Wang, Z. L. Environmental Energy Harvesting Adapting to Different Weather Conditions and Self-Powered Vapor Sensor Based on Humidity-Responsive Triboelectric Nanogenerators. *ACS Appl. Mater. Interfaces* **2019**, *11* (6), 6143–6153.
- (32) Tian, J.; Wang, F.; Ding, Y.; Lei, R.; Shi, Y.; Tao, X.; Li, S.; Yang, Y.; Chen, X. Self-Powered Room-Temperature Ethanol Sensor Based on Brush-Shaped Triboelectric Nanogenerator. *Research* **2021**, *2021*, 8564780.
- (33) Fu, X.; Xu, S.; Gao, Y.; Zhang, X.; Liu, G.; Zhou, H.; Lv, Y.; Zhang, C.; Wang, Z. L. Breeze-Wind-Energy-Powered Autonomous Wireless Anemometer Based on Rolling Contact-Electrification. *ACS Energy Lett.* **2021**, *6* (6), 2343–2350.
- (34) Zhao, T.; Xu, M.; Xiao, X.; Ma, Y.; Li, Z.; Wang, Z. L. Recent Progress in Blue Energy Harvesting for Powering Distributed Sensors in Ocean. *Nano Energy* **2021**, *88*, 106199.
- (35) Zhou, L.; Liu, D.; Liu, L.; He, L.; Cao, X.; Wang, J.; Wang, Z. L. Recent Advances in Self-Powered Electrochemical Systems. *Research* **2021**, *2021*, 4673028.
- (36) Wang, F.; Tian, J.; Ding, Y.; Shi, Y.; Tao, X.; Wang, X.; Yang, Y.; Chen, X.; Wang, Z. L. A Universal Managing Circuit with Stabilized Voltage for Maintaining Safe Operation of Self-Powered Electronics System. *iScience* **2021**, *24* (5), 102502.
- (37) Lei, R.; Shi, Y.; Ding, Y.; Nie, J.; Li, S.; Wang, F.; Zhai, H.; Chen, X.; Wang, Z. L. Sustainable High-Voltage Source Based on Triboelectric Nanogenerator with a Charge Accumulation Strategy. *Energy Environ. Sci.* **2020**, *13* (7), 2178–2190.
- (38) Wu, C.; Tetik, H.; Cheng, J.; Ding, W.; Guo, H.; Tao, X.; Zhou, N.; Zi, Y.; Wu, Z.; Wu, H.; Lin, D.; Wang, Z. L. Electrohydrodynamic Jet Printing Driven by a Triboelectric Nanogenerator. *Adv. Funct. Mater.* **2019**, *29* (22), 1901102.
- (39) Xu, L.; Wu, H.; Yao, G.; Chen, L.; Yang, X.; Chen, B.; Huang, X.; Zhong, W.; Chen, X.; Yin, Z.; Wang, Z. L. Giant Voltage Enhancement via Triboelectric Charge Supplement Channel for Self-Powered Electroadhesion. *ACS Nano* **2018**, *12* (10), 10262–10271.
- (40) Brandt, E. H. Suspended by Sound. *Nature* **2001**, *413* (6855), 474–475.
- (41) Abe, Y.; Yamamoto, Y.; Hyuga, D.; Awazu, S.; Aoki, K. Study on Interfacial Stability and Internal Flow of a Droplet Levitated by Ultrasonic Wave. *Ann. N. Y. Acad. Sci.* **2009**, *1161* (1), 211–224.
- (42) Abe, Y.; Hyuga, D.; Yamada, S.; Aoki, K. Study on Internal Flow and Surface Deformation of Large Droplet Levitated by Ultrasonic Wave. *Ann. N. Y. Acad. Sci.* **2006**, *1077* (1), 49–62.
- (43) Marzo, A.; Barnes, A.; Drinkwater, B. W. TinyLev: A Multi-Emitter Single-Axis Acoustic Levitator. *Rev. Sci. Instrum.* **2017**, *88* (8), 085105.
- (44) Marzo, A.; Corkett, T.; Drinkwater, B. W. Ultraino: An Open Phased-Array System for Narrowband Airborne Ultrasound Transmission. *IEEE Trans. Ultrason., Ferroelect., Freq. Contr.* **2018**, *65* (1), 102–111.
- (45) Ahn, J.; Xu, Z.; Bang, J.; Ju, P.; Gao, X.; Li, T. Ultrasensitive Torque Detection with an Optically Levitated Nanorotor. *Nat. Nanotechnol.* **2020**, *15* (2), 89–93.
- (46) Melde, K.; Mark, A. G.; Qiu, T.; Fischer, P. Holograms for Acoustics. *Nature* **2016**, *537* (7621), 518–522.
- (47) Zang, D.; Li, L.; Di, W.; Zhang, Z.; Ding, C.; Chen, Z.; Shen, W.; Binks, B. P.; Geng, X. Inducing Drop to Bubble Transformation via Resonance in Ultrasound. *Nat. Commun.* **2018**, *9* (1), 3546.
- (48) Guo, X.-Y.; Ma, Z.-C.; Liu, G.-W.; Li, D.; Tian, Q.-H. Adsorption of Re(VII) by Coated Solvent-Impregnated Resins Containing Alamine 304–1 from Sulfuric Acid Solutions. *Rare Met.* **2020**, *39* (8), 942–950.
- (49) Li, N.; Wu, L.; Yu, C.; Dai, H.; Wang, T.; Dong, Z.; Jiang, L. Ballistic Jumping Drops on Superhydrophobic Surfaces via Electrostatic Manipulation. *Adv. Mater.* **2018**, *30* (8), 1703838.
- (50) Watanabe, A.; Hasegawa, K.; Abe, Y. Contactless Fluid Manipulation in Air: Droplet Coalescence and Active Mixing by Acoustic Levitation. *Sci. Rep.* **2018**, *8* (1), 10221.
- (51) Seah, S. A.; Drinkwater, B. W.; Carter, T.; Malkin, R.; Subramanian, S. Correspondence: Dexterous Ultrasonic Levitation of Millimeter-Sized Objects in Air. *IEEE Trans. Ultrason., Ferroelect., Freq. Contr.* **2014**, *61* (7), 1233–1236.
- (52) Pang, H.; Liu, Y.; Li, J.; Yang, X. Solvothermal Synthesis of Nano-CeO₂ Aggregates and Its Application as a High-efficient Arsenic Adsorbent. *Rare Met.* **2019**, *38* (1), 73–80.
- (53) Zhang, S. P.; Lata, J.; Chen, C.; Mai, J.; Guo, F.; Tian, Z.; Ren, L.; Mao, Z.; Huang, P.-H.; Li, P.; Yang, S.; Huang, T. J. Digital Acoustofluidics Enables Contactless and Programmable Liquid Handling. *Nat. Commun.* **2018**, *9* (1), 2928.
- (54) Devaux, T.; Cebrecos, A.; Richoux, O.; Pagneux, V.; Tournat, V. Acoustic Radiation Pressure for Nonreciprocal Transmission and Switch Effects. *Nat. Commun.* **2019**, *10* (1), 3292.
- (55) Marzo, A.; Caleap, M.; Drinkwater, B. W. Acoustic Virtual Vortices with Tunable Orbital Angular Momentum for Trapping of Mie Particles. *Phys. Rev. Lett.* **2018**, *120* (4), 044301.
- (56) Gor'kov, L. On the Forces Acting on a Small Particle in an Acoustic Field in an Ideal Fluid. *Sov. Phys. - Dokl.* **1962**, *6* (1), 773.
- (57) Zang, D.; Yu, Y.; Chen, Z.; Li, X.; Wu, H.; Geng, X. Acoustic Levitation of Liquid Drops: Dynamics, Manipulation and Phase Transitions. *Adv. Colloid Interface Sci.* **2017**, *243*, 77–85.